

Missing monopole strength in ^{58}Ni and uncertainties in the analysis of α -particle scattering

G. R. Satchler

*Physics Division, Oak Ridge National Laboratory, Oak Ridge, Tennessee 37831
and Department of Physics & Astronomy, University of Tennessee, Knoxville, Tennessee 37996*

Dao T. Khoa

Department of Physics, Chung Yuan Christian University, Chung-Li, Taiwan 32023, Republic of China

(Received 23 July 1996)

Analyses of recent measurements of the scattering of alpha particles by ^{58}Ni at energies of 129 and 240 MeV have indicated that only about a third of the sum rule limit for isoscalar monopole transitions was found in the giant resonance region of excitation energies (E_x from 10 to 30 MeV). Here we examine the theoretical aspects of these analyses of inelastic scattering, both in the optical potentials obtained from elastic data and in the models used to represent the inelastic transitions. In particular we introduce the folding model and compare the use of folded optical and transition potentials with those obtained by deforming phenomenological optical potentials. We also study the effects of dynamic corrections on the folding interaction when this is density dependent. Both aspects are shown to have significant effects. We use more extensive elastic data at 139 and 340 MeV to illustrate the need for a density dependence in the folding interaction, as well as a need for different shapes for the real and imaginary parts of the potentials. Although these various features are shown to have non-negligible effects on the theoretical cross sections for the excitations at small angles, none of them is sufficient to account for all the apparently missing strength. We estimate, based upon the most realistic folding models, that about 50% of the sum rule limit for monopole excitation was observed within the two components of the spectra centered at 17.42 and 20.76 MeV. The sharing between these two components depends upon the assumptions made about the distribution of the giant dipole strength which also results in angular distributions that peak at 0° . Thus about one-half of the sum rule limit appears to have been observed, rather than the one-third originally inferred from these data using the deformed potential model. These conclusions are based, on the one hand, upon the spectral decomposition proposed for the results of the 240 MeV experiment and, on the other hand, upon assuming that the simple breathing mode form is adequate for the monopole transition densities. The results may be sensitive to deviations from either assumption. In a similar way we also infer that at least 55%, and perhaps as much as 70%, of the isoscalar quadrupole sum rule limit may be present in this giant resonance range of excitation energies in ^{58}Ni . [S0556-2813(97)01501-X]

PACS number(s): 24.30.Cz, 24.10.-i, 25.55.Ci, 27.40.+z

I. INTRODUCTION

The location and strength (or even the existence) of the giant isoscalar monopole resonance (GMR) in the lighter nuclei ($A < 90$, say) remain a somewhat controversial question. Studies of the inelastic scattering of alpha particles by ^{24}Mg and ^{28}Si have indicated that its strength is strongly fragmented in these two nuclei and distributed over a range of excitation energies of at least 8–9 MeV [1,2]. About 30% of the monopole energy-weighted sum rule (EWSR) was identified in $^{64,66}\text{Zn}$ using alpha particles of 129 MeV [3].

Measurements on ^{58}Ni have also been made by two groups using 152 MeV alpha particles [4,5]. The first group [4], following an earlier analysis of some (p, p') data [6], assumed a GMR peak at an excitation energy of 20.0 ± 0.5 MeV. This interpretation was challenged by Garg *et al.* [7], who showed that the angular distribution for the purported GMR peak was consistent with a quadrupole excitation. A reanalysis of their own data taken with 129 MeV alpha particles [3] led to the same conclusion. The second group using 152 MeV alpha particles [5] concluded that the best fit to their spectra in the giant resonance region was obtained with three Gaussian peaks, with the GMR peak at 17.31 ± 0.20 MeV, very close to a giant quadrupole resonance (GQR) at

16.39 ± 0.22 MeV, and a subsidiary peak at an excitation of 20.18 ± 0.23 MeV. The strength of the GMR peak was found to exhaust only $(23 \pm 5)\%$ of the isoscalar-monopole energy-weighted sum rule, while the GQR peak was assigned $(38 \pm 8)\%$ of its EWSR.

An additional experiment with 129.5 MeV alphas was performed [8], followed more recently by measurements using alpha particles of 240 MeV [9]. Again the spectra were decomposed into three main Gaussian peaks, supplemented by two weaker and narrower ones to accommodate the structure seen on the low excitation energy side of the giant resonance region. The excitation energies and strengths found for the three main peaks seen in these two experiments were in general agreement with each other and with those extracted by Duhamel *et al.* [5]. The experiment at the highest energy of 240 MeV [9] yielded the greatest peak-to-background ratio at small scattering angles, as well as removing the broad pickup-breakup contributions, due to the formation and decay of ^5Li and ^5He , to excitation energies above 40 MeV. Peak fitting of the resulting spectra in the giant resonance region of $E_x < 30$ MeV was interpreted as evidence for 44% of the quadrupole EWSR at $E_x = 16.08$ MeV and 22% of the monopole EWSR at $E_x = 17.42$ MeV, mixed with 7% of the quadrupole. A peak at higher excitation, $E_x = 20.76$ MeV,

was fitted with 10% of the monopole EWSR, 7% of the quadrupole, and 100% of the isovector giant dipole resonance.

An important feature of measurements of monopole excitations by alpha particles is to approach as closely as possible to 0° , where the monopole angular distribution has its maximum. Furthermore, the monopole distribution is predicted to exhibit a deep, narrow minimum following the 0° maximum. These two features most easily distinguish it from the distributions for other multipolarities [3]. The measurements reported in [4] were for angles greater than 5° , beyond the first minimum for monopole excitations, while those reported in [5] extended into 1.3° , thus covering the minimum and a substantial part of the forward peak. The data from the Texas A & M cyclotron include scattering to 0° [3,7–9], and thus provide the most stringent limits on the monopole strength.

This brief review of measurements on ^{58}Ni indicates a consensus that a substantial portion (about one-half) of the quadrupole EWSR is located around an excitation energy of 16 MeV, while only about 30% of the monopole EWSR is found in the region $E_x \approx 10\text{--}30$ MeV. However, there are uncertainties associated with these conclusions which might be classified as “experimental” or “theoretical.” The “experimental” uncertainties include those arising from the decomposition of the peaks observed in the giant resonance region of the spectra (including the subtraction of the “background”). For example, the use of symmetric Gaussian shapes may be questioned when only 20% or so of the EWSR is observed. This implies considerable fragmentation of the resonance. Theoretical calculations using the random phase approximation (RPA) [10] support this fragmentation, but with a distribution in excitation energy of the fragments that is not symmetric.

The “theoretical” uncertainties include the theoretical models used to analyze the experimental results and extract from them a measure of how much the EWSR has been exhausted. In particular one may question the use of the deformed potential model. These concerns are the principal motivation of the present paper. We concentrate on alpha particles with 240 MeV bombarding energy because it is for these that the most precise and extensive data are available [9].

II. THEORETICAL MODELS

Before accepting that a majority of the monopole strength in ^{58}Ni is “missing” from the expected giant resonance region of excitation energies, it is important to know to what extent this result depends upon the theoretical assumptions made when interpreting the data. It is assumed, of course, that the inelastic scattering is a direct reaction [11], and it has been confirmed that the distorted-wave Born approximation, which treats the coupling interaction to first order, gives results almost identical to a full solution of the coupled-channels (CC) problem, showing that higher-order effects are either not important or are adequately represented by the optical potentials used. (In practice, we find it more convenient to use the CC approach and this was done for the results reported here. An effective bombarding energy and effective masses were used at each energy [12] to ensure the

relativistically correct center-of-mass momentum and Sommerfeld parameter.)

A. Deformed potential model

It remains for the interaction potentials to be defined. The results referred to in the Introduction were obtained using the deformed potential (DP) model. In this approach, a complex optical potential $U(r)$ (usually having a Woods-Saxon shape) is found by fitting the observed elastic scattering. This potential is then deformed to provide parts which model the transition potentials needed to describe the inelastic scattering. The transition potential for excitation of a one-phonon vibrational state with multipolarity $l \geq 2$ has a radial part given by (we use the notation and normalization of [13])

$$G_l^{\text{DP}} = -\delta_l^U dU(r)/dr. \quad (2.1)$$

The amplitude (“deformation length”) δ_l^U is adjusted to match the observed inelastic cross sections. As written here, we have assumed that the real and imaginary parts of the potential U have the same deformation length δ_l^U .

A breathing mode is assumed for monopole ($l=0$) excitations [14,15] with a transition potential

$$G_0^{\text{DP}}(r) = -\alpha_0^U [3U(r) + rdU(r)/dr]. \quad (2.2)$$

Again the amplitude α_0^U is assumed to be the same for the real and imaginary parts of U . It is adjusted to match the measured cross sections. The problem that then arises is to relate these *potential* amplitudes to the multipole moments of the corresponding transition *densities* of the nucleus being excited. Frequently, this is done by assuming that the nuclear density is deformed in the same way as the optical potential and with the same deformation length [16]. In this way, the surfaces of the density and of the potential are displaced by the same distance. Although perhaps intuitively appealing, there is no theoretical justification for this procedure [17,18], particularly for the monopole breathing mode. The treatment of the imaginary part of the coupling in this way is especially questionable. Although the imaginary coupling is not dominant, neither is it negligible.

B. Folded potential models

It has been reemphasized recently [16,18,19] that the folding model approach to the potentials is more basic and provides a direct and unambiguous link between the potentials and the underlying nuclear densities. It can also lead to results that differ significantly from those obtained using the DP model. A recent example used this fact to explain an apparent “hindrance” of 3^- excitations (by factors of 2–3) by the scattering of ^{17}O ions [20].

In this approach, the potentials (optical and transition) are generated by folding an effective nucleon-nucleon interaction v over the density distributions of the target and projectile [19]. The ground-state densities needed for generating the optical potential are usually known well enough, but, of course, the folding approach for the transition potential depends upon having a reliable model for the transition density of the nucleus being excited. Other analyses (for example, [21]) have provided support for the use of the collective

Bohr-Mottelson (BM) form of the transition density for the excitation of low-lying ‘‘vibrational’’ states with $l \geq 2$,

$$g_l^{\text{BM}}(r) = -\delta_l^m d\rho_l(r)/dr, \quad (2.3)$$

where $\rho_l(r)$ is the ground-state density of the nucleus being excited and δ_l^m is the corresponding matter deformation length. By extension, one would expect this to be a good choice also for the giant multipole resonances with $l \geq 2$.

The breathing mode form for the GMR transition density is

$$g_0(r) = -\alpha_0^m [3\rho_l(r) + r d\rho_l(r)/dr]. \quad (2.4)$$

Although a plausible choice, there is unfortunately no independent experimental support for this form. Theoretical structure calculations using the RPA tend to give transition densities similar to this; on the other hand, when fragmentation of the GMR is present, the various fragments may be associated with different forms. For example, theoretical RPA transition densities and their associated folded potentials for two GMR fragments in ^{60}Ni are shown in [10]. One fragment yields results close to Eqs. (2.4) and (2.2), respectively, while the shapes for the other fragment are significantly different.

This kind of uncertainty can be critical for the scattering of projectiles that are relatively strongly absorbed, for these are strongly dependent upon the tails of the transition potentials in the vicinity of the strong absorption radii. (The strong absorption radius for 240 MeV alphas on ^{58}Ni is between 6 and 7 fm.) Reference [10], which examines the GMR in four targets excited by 152 MeV alpha particles, suggests that the use of the model (2.4) could lead to estimates of the total monopole strength which are (10–30)% larger than would be given by using the RPA transition densities. However, in the absence of a suitable alternative for ^{58}Ni , we continue to use the form (2.4) in this paper.

The representation of the imaginary coupling also presents a problem in the folding approach. Simply assuming that the nucleon-nucleon interaction has a complex strength, determined by the elastic scattering, provides a straightforward procedure which results in the real and imaginary transition potentials having the same radial shape. This appears to have had some success [16,20] in some circumstances, despite the lack of theoretical justification. However, in many cases (including alpha-particle scattering at $E \geq 100$ MeV), this assumption is known to be unrealistic for the elastic scattering and prevents one from obtaining satisfactory fits to measurements taken at angles beyond the Fraunhofer diffraction region. An example for $\alpha + ^{58}\text{Ni}$ scattering is provided in [22]. [Our own work, described in Sec. III A and shown in Fig. 2(a) below, provides another example.] Then an alternative solution frequently used is a hybrid model in which the real interaction is folded and the imaginary part is treated phenomenologically such as by a Woods-Saxon potential. The imaginary inelastic coupling is then generated by deforming this potential, as in the DP model. This leaves the corresponding deformation length undefined. For $l \geq 2$ it is frequently set equal to the density deformation length, and we do that here. The best choice for the monopole breathing mode is much less obvious.

C. Effective interaction and density dependence

The other important ingredient of the folding model is the effective nucleon-nucleon interaction. The simplest approach, known as single folding and used primarily for alpha particles at lower energies (≤ 100 MeV, say), is to average this interaction over the density distribution of the alpha particle and represent the result by a simple functional form $\bar{v}(s)$. The most popular form is a Gaussian with a complex strength [4,23],

$$\bar{v}_G(s) = -(v + iw)\exp(-s^2/t^2), \quad (2.5)$$

where $s = |\mathbf{r} - \mathbf{r}'|$ is the distance between the center of mass of the alpha particle and a target nucleon. The range t is about 2 fm; we adopt the value $t = 1.94$ fm from a study of elastic data at forward angles for 140 MeV alpha particles [4]. The strengths v and w are adjusted to optimize the agreement with elastic measurements at each energy.

While the simple model (2.5) will reproduce the measured scattering at forward angles, even at 240 MeV where the data extend only to 17° [24], it has long been known to be inadequate at energies ≥ 100 MeV when data are available for a more extended angular range that displays rainbow scattering [25]. The model (2.5) is deficient in two ways. First, it assumes that the real and imaginary parts of the optical potential have the same radial shape. This results in much too strong absorption in the interior. We avoid this by a hybrid model in which the imaginary potential is represented by a Woods-Saxon shape or its square, which differs from the shape of the real folded potential. Second, the strength v of the real interaction which gives the peripheral potential required to fit the small-angle diffractive scattering results in a potential that is too deep in the interior to reproduce correctly the rainbow features at large angles. This can be corrected by making the interaction between the alpha particle and target nucleon depend upon the density of the nuclear matter in which they are immersed. The requirement that nuclear matter saturate ensures that this density dependence (DD) reduces the strength of the interaction as the density increases, weakening the folded potential in the interior while leaving the peripheral values largely unchanged. We used a popular form of DD,

$$\bar{v}_{\text{DDG}}(s, \rho) = \bar{v}_G(s) f(\rho), \quad (2.6a)$$

with

$$f(\rho) = 1 - \alpha \rho(r')^\beta, \quad \beta = 2/3, \quad (2.6b)$$

where $\rho(r')$ is the ground-state density of the target nucleus at the position r' of the target nucleon. A good fit to elastic data was found (see below) with $\alpha = 1.9 \text{ fm}^2$, associated with a Gaussian \bar{v}_G with a range $t = 1.88$ fm.

An additional consistency feature arises when a density-dependent interaction like Eqs. 2.6 is applied to inelastic scattering [26,27]. A deformation of the density $\rho \rightarrow \rho + \delta\rho$ also affects the interaction $v(\rho) \rightarrow v(\rho + \delta\rho)$. To lowest order this is included by using the modified interaction

$$v'(\rho) = v(\rho) + \rho \delta v(\rho) / \delta \rho; \quad (2.7a)$$

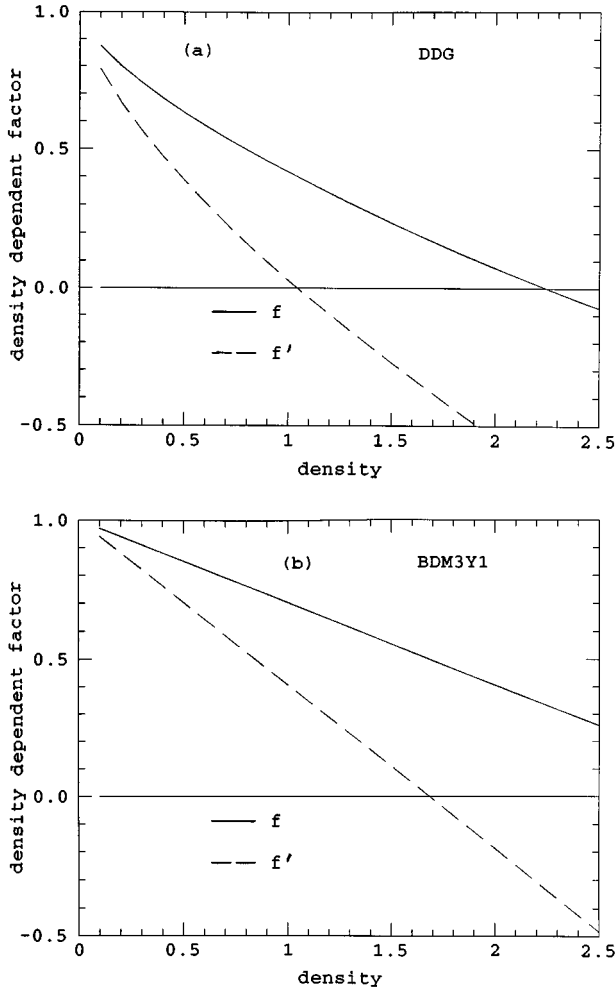


FIG. 1. The density-dependent factor $f(\rho)$ associated with (a) the Gaussian single-folding interaction DDG and (b) the M3Y double-folding interaction BDM3Y1. Also shown (dashed curves) are the $f'(\rho)$ factors when the dynamical correction (2.7) for inelastic scattering is included. The density is given in ratio to the density $\rho_0 = 0.17 \text{ fm}^{-3}$ of normal nuclear matter.

indeed, this is exact for the excitation of one phonon of a harmonic shape vibration [27]. In the case of Eq. (2.6b), this corresponds to replacing α by $\alpha' = \alpha(1 + \beta) = (5/3)\alpha$, so that $f(\rho)$ is replaced by

$$f'(\rho) = 1 - \alpha(1 + \beta)\rho(r')^\beta. \quad (2.7b)$$

The correction (2.7) further reduces the interaction strength inside the target nucleus, as indicated in Fig. 1.

Finally, we return to double folding, namely, the explicit use of a realistic density-dependent nucleon-nucleon interaction folded over the density distributions of both the target nucleus and the alpha particle. For our purpose we adopt a very recent interaction called BDM3Y1 (Paris) which has already been shown to give a good account of refractive alpha-particle scattering at energies ranging from 59 to 172 MeV [28]. It is based upon a G matrix derived from the Paris nucleon-nucleon potential. It has a linear dependence on density [corresponding to $f(\rho) = 1 - \alpha\rho$, or $\beta = 1$, in Eq. (2.6b)], adjusted to give saturation of nuclear matter at the correct density and binding energy [28,30]. This required

$\alpha = 1.7452 \text{ fm}^3$. It yields an incompressibility for nuclear matter of $K = 270 \text{ MeV}$. This interaction incorporates an accurate local approximation to knock-on exchange effects, an important consideration because these exchange contributions dominate over the direct ones for the Paris potential [28]. The single-folding approach, using alpha-nucleon interactions such as Eq. (2.5) or Eqs. (2.6), does not consider knock-on exchange explicitly. It is assumed that exchange effects are taken into account implicitly when adjusting the interaction to reproduce the observed elastic scattering. This may be adequate for monopole inelastic scattering, since elastic scattering itself is a monopole transition, but it ignores the possibility for higher multipoles that the effective interaction should be multipole dependent because of exchange effects.

A Gaussian form was chosen for the alpha-particle density distribution [28],

$$\rho_\alpha(r) = 0.4229 \exp(-0.7024r^2), \quad (2.8)$$

which has a rms radius of 1.461 fm, consistent with electron scattering measurements of the charge radius [29]. The explicit form of the BDM3Y1 interaction and its parameter values are given in [28]. The density dependence of BDM3Y1 is also shown in Fig. 1; again, the dynamical correction (2.7) further suppresses the interaction at small radii. The density dependence of BDM3Y1 is less severe than that for the single-folding interaction DDG because the latter already implicitly contains in an average way the effects of the density of the projectile alpha particle.

D. Sum rule limits

Certain linearly energy-weighted sum rules (EWSR's) for the operators $r^l Y_l^m(\theta, \phi)$ (for $l \geq 2$) and r^2 (for $l = 0$) acting on the target nucleus ground state, expressions for which are given in Ref. [16], for example, provide convenient measures of the strength of transitions exciting giant resonances. For example, if the Tassie transition density (2.4) is appropriate for all monopole excitations, the sum rule provides a limitation on their amplitudes α_{0i}^m ,

$$\sum_i (\alpha_{0i}^m)^2 E_{xi} = 4A (\hbar^2/2m) \langle r^2 \rangle_m, \quad (2.9)$$

where α_{0i}^m is the amplitude for the monopole state with excitation energy E_{xi} and $\langle r^2 \rangle_m$ is the mean square radius of the ground state. (We use $\hbar^2/2m = 20.735 \text{ MeV fm}^2$.) The operators involved here are similar to those for the electric excitation of the target protons in the long-wavelength limit. However, it is appropriate to point out that excitation by the inelastic scattering of hadrons is associated with a radial dependence different from r^l (or r^2 for $l = 0$), although in both cases the operators emphasize contributions from the target nucleus surface (see Chap. 14 of Ref. [11]). Thus the sum rule expressions may be expected to provide only a qualitatively reliable guide to hadronic cross sections. Hence it should be borne in mind that, for example, two transition densities that have the same r^l (or r^2 for $l = 0$) moment (and thus the same fraction of the corresponding EWSR) may give rise to significantly different hadronic cross sections, particularly when the hadron is susceptible to strong absorption and thus is sensitive to the *tail* of the transition potential.

Resolution of this problem requires independent information, experimental or theoretical, about the appropriate transition density. Unfortunately, this is especially difficult to obtain for monopole excitations.

III. APPLICATIONS TO ELASTIC SCATTERING

We use the ability of a given interaction to reproduce the observed elastic scattering as a criterion of its validity and to determine the optimum values of its parameters. The real part of the optical potential was generated using the folding model. A two-parameter Fermi distribution was used for the ground state of ^{58}Ni , with a radius of 4.08 fm and surface diffuseness of 0.515 fm. This has a rms radius of 3.695 fm, very close to that deduced from high energy proton scattering [31].

A. Single folding and density dependence

There are elastic data for the scattering of 139 MeV alpha particles from ^{58}Ni which extend out to 80° and display a well-developed rainbow [32]. Figure 2(a) shows the best fit to these data that could be obtained using either the density-independent interaction (2.5) or the density-dependent form (2.6) with a complex strength, so that the real and imaginary potentials have the same radial shape. Both fits are unacceptable. However, excellent agreement, shown in Fig. 2(b), is obtained by including both density dependence and an imaginary potential with a different shape. The density-dependent Gaussian (DDG) forms (2.5) and (2.6) were used for the real potential, with $v=53.95$ MeV, $w=0$, $\alpha = 1.9$ fm², and $t=1.88$ fm. The imaginary potential was taken to have a Woods-Saxon shape,

$$\text{Im}U(r) = -W/(e^x + 1), \quad x = (r - R_W)/a_W, \quad (3.1)$$

with $W = 17.3$ MeV, $R_W = 6.238$ fm, and $a_W = 0.646$ fm. (An almost indistinguishable fit is obtained by using the square of the Woods-Saxon shape.)

Extensive data displaying refractive features are also available at the higher energy of 340 MeV [33]. These were studied to provide some indication of the variation of the interaction with bombarding energy so that interpolation to 240 MeV or extrapolation to 129.5 MeV could be performed. An optimum fit [Fig. 2(c)] was obtained with the same DDG interaction used at 139 MeV, except for a reduction in strength to $v=39.8$ MeV. The accompanying Woods-Saxon imaginary potential was similar except for a somewhat more diffuse surface ($W=16.8$ MeV, $R_W=6.269$ fm, and $a_W=0.765$ fm).

The volume integrals per interacting pair of nucleons for the real potentials, $J_R=282$ MeV fm³ ($E=139$ MeV) and $J_R=208$ MeV fm³ ($E=340$ MeV), are consistent with those obtained from a global study [34] which included these data, as well as others taken at $E=104$ and 288 MeV. The results indicate a dependence on energy that is close to linear over this range (albeit a little curvature is to be expected from dispersion relation considerations [34]). Hence it is surprising that fits to the 240-MeV data [24] result in real potentials that are approximately 20% or more weaker than expected from interpolation between the other two energies. This occurs whether the potentials used are phenomenological

Woods-Saxon ones (see Fig. 4 in [24]), single-folded ones, or (see below) obtained from double folding. The data at 240 MeV extend only to 17° in angle, covering the forward-angle diffractive region of the angular distribution. This indicates that the *observed* scattering is primarily sensitive to the potential in the surface and that the interpolated potentials are too strong in this region. They yield a diffractive pattern that is slightly shifted forward in angle, compared to that observed.

It is easy to obtain a good fit to the more limited elastic data at 240 MeV. That shown in Fig. 3 is a typical example which uses the DDG interaction for the folded real potential with a strength of $v=36.15$ MeV (compared with the $v \approx 46.8$ MeV, which is suggested by linear interpolation between the values obtained at 139 and 340 MeV). The optimum Woods-Saxon imaginary part has $W=35.25$ MeV, $R_W=4.810$ fm, and $a_W=0.926$ fm (whereas interpolation would suggest $W \approx 17$ MeV, $R_W \approx 6.25$ fm, and $a_W \approx 0.70$ fm). It is possible to obtain an acceptable fit with the expected $v=46.8$ MeV (albeit with a χ^2 almost 3 times as large), but only by introducing a very strongly absorptive imaginary potential ($W \approx 150$ MeV). It would not be possible to reproduce the 139 and 340 MeV large-angle data with such a potential. Later we shall examine what effect this uncertainty has upon the predictions for the inelastic scattering at $E=240$ MeV.

B. Double folding

Double-folded potentials were also constructed using the BDM3Y1 (Paris) interaction described earlier. These are energy dependent. This energy dependence arises mostly from the explicit treatment of the knock-on exchange contributions but includes a weak phenomenological linear dependence [28]. Thus the real potential is fully determined *a priori*, although we include an overall renormalization factor N which is adjusted to optimize the fit to the measurements. N should be close to unity in order for this procedure to be meaningful. Again we use the Woods-Saxon model (3.1) for the imaginary potential, adjusting the parameter values for best agreement.

Excellent fits to the 139- and 340-MeV data were obtained, very similar to those shown in Figs. 2(b) and 2(c). Renormalization factors a little larger than unity were required ($N=1.18$ at $E=139$ MeV and $N=1.23$ at $E=340$ MeV), as is typical for alpha particle scattering [28,34]. The optimum imaginary potential at 139 MeV had $W=22.9$ MeV, $R_W=5.672$ fm, and $a_W=0.797$ fm. The corresponding values at 340 MeV were $W=34.6$ MeV, $R_W=5.358$ fm, and $a_W=0.691$ fm. The real volume integrals were $J_R=267$ MeV fm³ ($E=139$ MeV) and $J_R=195$ MeV fm³ ($E=340$ MeV).

A discrepancy similar to that described above was encountered when this double-folded potential was applied to the measurements at 240 MeV. The optimum fit is indicated by the dashed curve in Fig. 3. A renormalization factor *less* than unity, $N=0.96$, was required in order to match the observed diffraction pattern, rather than the value $N \approx 1.2$ expected by interpolation between the other two energies. The accompanying imaginary Woods-Saxon potential had $W=45.6$ MeV, $R_W=4.361$ fm, and $a_W=0.995$ fm. Just as

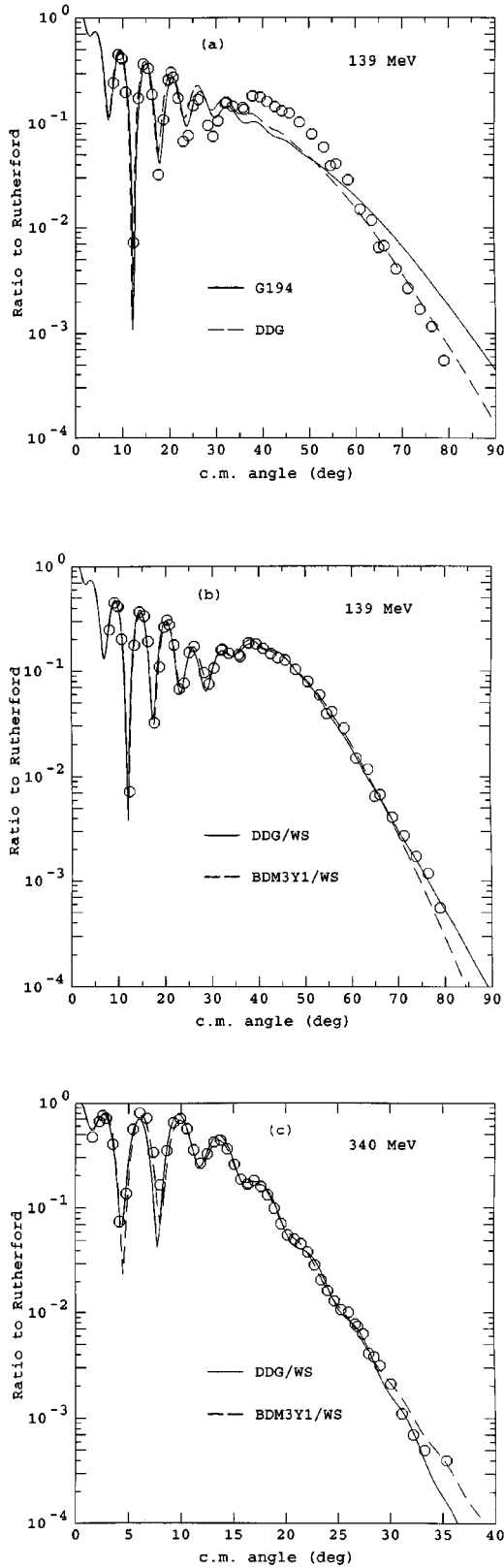


FIG. 2. (a) The best fits to elastic data for 139 MeV alpha particles on ^{58}Ni [32] that are obtainable using folded potentials with a Gaussian (G194) or a density-dependent Gaussian (DDG) interactions with complex strengths, so the real and imaginary parts have the same shape. (b) The same data fitted by density-dependent interactions for the real potentials and Woods-Saxon shapes for the imaginary potentials. (c) As in (b), applied to data taken at 340 MeV [33].

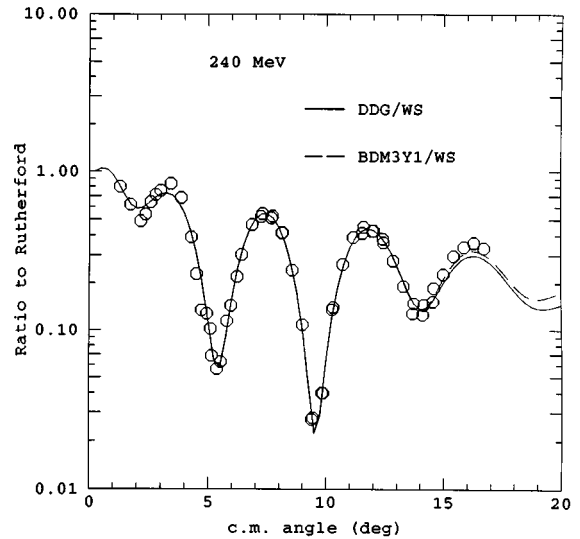


FIG. 3. Fits to the elastic data for 240 MeV alpha particles on ^{58}Ni [24] using a single-folded real potential with a density-dependent Gaussian interaction (DDG) or a double-folded real potential with an M3Y-type interaction (BDM3Y1), both accompanied by a Woods-Saxon imaginary potential.

with single folding, an acceptable fit (but with χ^2 twice as large) could be obtained with $N=1.2$ but accompanied by a very strongly absorptive imaginary potential.

IV. APPLICATIONS TO INELASTIC SCATTERING

A. Low excited 2^+ and 3^- states of ^{58}Ni

For calibration purposes, we study here the 240-MeV data [24] for exciting the lowest 2^+ and 3^- bound states of ^{58}Ni . First we compare folding with the use of the deformed (Woods-Saxon) potential to generate the transition potentials. Then, within the folding model we compare the use of density-dependent and density-independent interactions, and study the effects of the dynamical corrections (2.7). In each case the models used are required to give equivalent fits to the elastic data.

The ‘‘adopted’’ experimental values [35,36] for the electric transition rates are $B(E2) = 0.070 e^2 b^2$ and $B(E3) = 0.017 e^2 b^3$. We may extract matter deformation lengths if we use the BM model (2.3) for the transition densities and simply assume that the neutron and proton densities are in the ratio of N/Z and have equal deformation lengths. Then we find $\delta_2^m = 0.847$ fm and $\delta_3^m = 0.857$ fm. We further assume that these equal the potential deformation lengths, $\delta_i^m = \delta_i^U$, when we compare folding with the DP model (2.1), or in the hybrid model where the real potential is obtained by folding and a Woods-Saxon form is used for the imaginary potential.

In each case, Coulomb excitation was included using the $B(E1)$ values mentioned above.

We adopted the Woods-Saxon potential from [24] for the DP calculations. The various single-folding models gave peak cross sections for the quadrupole excitation that were about 20% smaller than those obtained using the DP model with the same deformation length. Figure 4 compares the DP predictions to those of the folding model using the real DDG interaction described in the preceding section (with $v=36.15$ MeV), and including the correction (2.7) for the

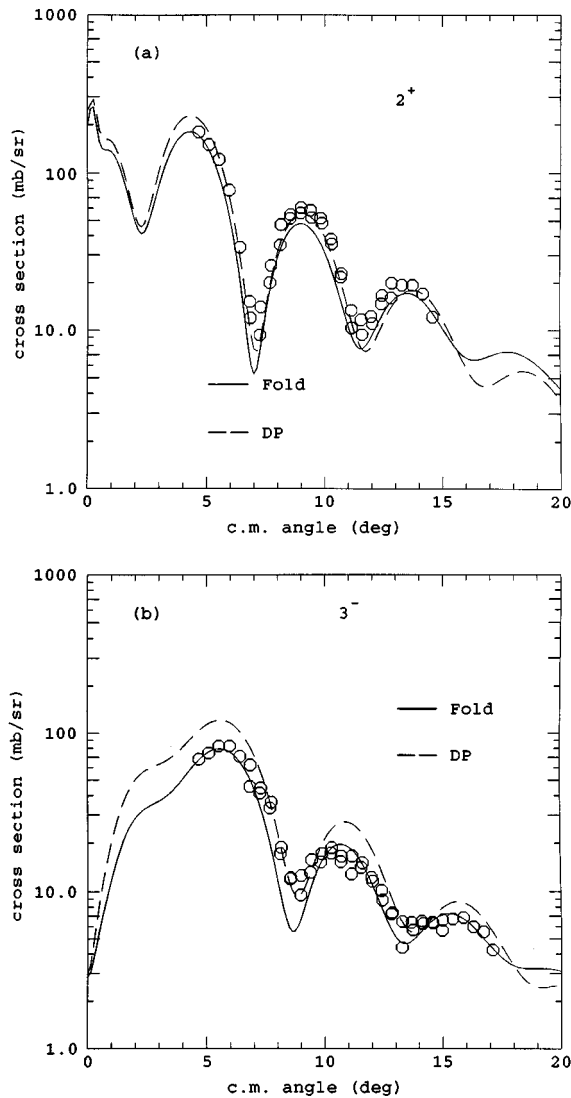


FIG. 4. Comparison of folding model predictions, using the density-dependent interaction DDG, for exciting the lowest excited states in ^{58}Ni by 240 MeV alpha particles, with those using the deformed potential (DP) model based upon the Woods-Saxon potential of [24]. (a) The 2^+ state at $E_x = 1.454$ MeV with $B(E2) = 0.070 e^2 b^2$, corresponding to a deformation length of $\delta_2 = 0.847$ fm. (b) The 3^- state at 4.475 MeV with $B(E3) = 0.017 e^2 b^3$, corresponding to a deformation length of $\delta_3 = 0.857$ fm.

inelastic coupling. The deformed Woods-Saxon model was used for the imaginary interaction. The DP model gives a good fit to the measurements [24], while the folding model fit is improved if its deformation length is increased by about 10%. This may be an indication that the appropriate neutron deformation length is a little larger than that for the protons, or it may reflect an uncertainty in the $B(E2)$ value.

The situation is different for the octupole excitation, where the DP model predicts cross sections that are 50% larger than the folding models for a given deformation length. Figure 4 shows that folding, with the deformation length deduced from the $B(E3)$ value, gives good agreement with the measurements [24], while the DP model predicts cross sections that are too large. (This is similar to a previous finding for octupole excitations by heavy ions [20]. Such discrepancies are strongly dependent on the multipolarity l ,

increasing as l increases when it is assumed that the matter and potential deformation lengths are equal [19].)

This deficiency of the DP model raises an interesting question when we use the hybrid folding model (folded real potential plus Woods-Saxon imaginary potential), which is needed when data at large angles are to be fitted. We have used the DP model to estimate the contribution from the imaginary potential to the inelastic scattering. Now there is reason to suspect that this provides an overestimate by an amount that depends upon the multipolarity of the transition. The imaginary contribution is not negligible, and typically increases the cross sections by about 50% compared to using the real interaction alone. Fortunately, the various versions of the folding models (hybrid or folded imaginary) predict cross sections at forward angles that are within a few percent of each other, implying that this uncertainty is not a large source of error in the present case. This similarity at forward angles also holds whether or not one includes a density dependence in the interaction. However, this need no longer be true if one were attempting to fit data over a larger range of scattering angles.

The dynamic correction (2.7), needed when the interaction is dependent on the density, reduces even further the strength of the transition potential in the interior of the target, as indicated in Fig. 1. Its effect on the inelastic scattering can be large. In the present case, omitting it increases the predicted inelastic cross sections by about 35% without changing the angular distributions significantly. (The increase is found to be somewhat less for 139 MeV alpha particles, being about 25%.)

Furthermore, there is a general rule for small-angle scattering, that two interactions that give the same elastic scattering will also give very similar inelastic scattering. This rule is only obeyed when comparing density-dependent and density-independent interactions if the dynamic correction (2.7) is included for the former.

It was reported in the preceding Section that interpolation between the fits to the elastic data at 139 and 340 MeV implies that the real interaction should be about (20–30)% stronger than was used for the results illustrated in Fig. 4. We checked the possible effects of this by repeating the calculations with the interpolated potentials. The cross sections do not simply increase as the square of the interaction strength, partly because the imaginary interaction also changes, and partly because the elastic scattering (the “distorted waves”) are affected as well as the inelastic coupling. We find that the peak cross sections for both 2^+ and 3^- are increased by about 10%, with small changes in the angular distributions (mainly a slight shift of a few percent to smaller angles in a way analogous to that seen for the elastic scattering) which worsen the agreement with the data seen in Fig. 4.

B. Giant monopole excitations

Here we examine the effects of the various models on $l=0$ isoscalar monopole excitations. We assume the breathing mode form (2.4) for the transition density. The Fermi ground state density that was used to generate the folded optical potentials has a rms radius of 3.695 fm. If an excitation energy of 17.42 MeV is assumed for the giant monopole

resonance (GMR), 100% of the energy-weighted sum rule limit is exhausted by an amplitude of $\alpha_0^m=0.1374$, corresponding to a reduced transition rate of $B(IS, l=0)=0.377 b^2$ [20].

In order to apply the DP model we use the form (2.2) for the transition potential, as was done in [8]. It is not obvious how to relate the potential amplitude α_0^U to the amplitude α_0^m of the underlying matter oscillation to which the sum rule limit applies. This relation needs to be defined before we can make a meaningful comparison of the the folding and DP models. Earlier, when making this comparison for higher multipole excitations, we assumed that the matter and potential deformation lengths were equal. In the same spirit, it is plausible to equate the displacements at the corresponding matter and real potential radii [20], giving

$$\alpha_0^U R_V = \alpha_0^m c, \quad (4.1)$$

where R_V is the radius of the real part of the Woods-Saxon potential and c is the matter radius of the target ground state. Here, $c=4.08$ fm, while $R_V=4.75$ fm for the DP model. Nonetheless, this remains a particular source of uncertainty for the application of the DP model to breathing mode excitations; note, for example, that the DP cross sections are proportional to the square of α_0^U .

An analogous prescription is used for the imaginary interaction in the hybrid model (folded real interaction, Woods-Saxon imaginary part), namely, Eq. (4.1), with R_V replaced by R_W .

First we compare the predictions of the DP model [9] with those obtained from the most sophisticated folding models considered here, namely, those using the density-dependent DDG (single-folding) and BDM3Y1 (Paris) (double-folding) interactions for the real potentials and phenomenological Woods-Saxon forms for the imaginary potentials. The cross sections are shown in Fig. 5 for excitation of a monopole state at 17.42 MeV which exhausts 100% of the sum rule limit (2.9). [It should also be remembered that these results depend upon assuming the relation (4.1) and its counterpart in the folding model, not to mention the dependence upon using the ansatz (2.2) for the transition potential in the DP model and Eq. (2.4) for the transition density in the folding approach.] Values of the cross sections are also given in Table I for representative angles; 1° is the smallest (average) angle for which measurements are available [9] while 5° is the location of the second peak in the monopole angular distribution. The entries in this table also give some indication of the dependence upon Q value.

The two folding models give cross sections that differ by only a few percent. The results from the DP model, using the Woods-Saxon potential from [24], fall between those for the folding model at the most forward angles, but rise above both of them at larger angles (by about 20% on the second peak at 5°). The reason for the relative insensitivity of the monopole cross sections to the model used is clarified by Fig. 6, which shows the corresponding transition potentials. There are dramatic differences in the nuclear interior, but the various potentials become much closer at the important larger distances in the vicinity of the strong absorption radius (which is about 7 fm in this case). Since the measured cross section near 1° is dominated by the monopole excitation, we

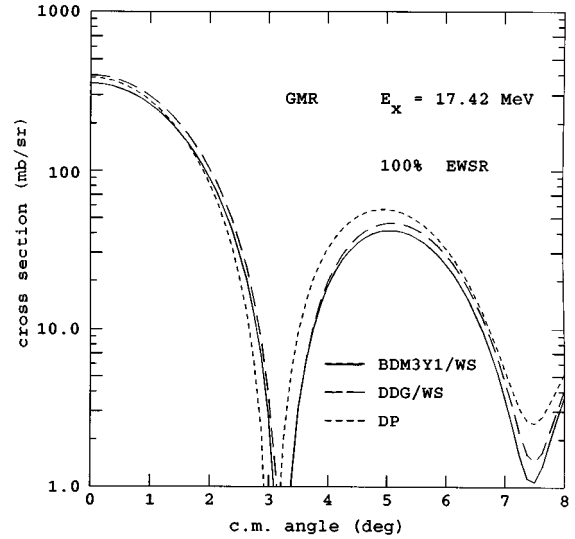


FIG. 5. Differential cross sections at forward angles for 240 MeV alpha particles exciting a giant monopole resonance at 17.42 MeV in ^{58}Ni that exhausts 100% of the energy-weighted sum rule. The predictions of the deformed potential (DP) model, based upon the Woods-Saxon potential of [24], are compared to predictions using folding models for the real parts of the transition potentials and deformed Woods-Saxon potentials for the imaginary parts. DDG is the density-dependent single-folding Gaussian interaction, and BDM3Y1 is the density-dependent double-folding M3Y-type interaction.

see immediately that there is little opportunity for the use of the folding model, as defined here, resulting in a measure of the sum rule depletion by the monopole excitation that is very much larger than that arrived at originally [9].

Other choices for the effective interaction, which fit the 240 MeV elastic data but ignore the constraints implied by the wide-angle data at 139 and 340 MeV (namely, the need for density dependence and a different shape for the imaginary potential), may result in monopole cross sections that differ by larger amounts. For example, we may take the simple Gaussian of Eq. (2.5) with a complex strength and range $t=1.94$ fm, as was used earlier [4]. This gives a good fit to the 240 MeV elastic scattering with $v=24.9$ MeV and $w=14.95$ MeV. The corresponding monopole transition potential is included in Fig. 6. The theoretical monopole inelastic cross sections given by using this (Table I) are then about 30% smaller than those obtained using the more realistic density-dependent Gaussian with a Woods-Saxon imaginary part that we have denoted DDG, and hence would imply a depletion of the sum rule limit that is nearly 40% greater.

Attention was drawn earlier to a discrepancy between the optimum potential fits to the elastic data at 240 MeV and the potentials expected by interpolation between fits to data at 139 and 340 MeV. Consequently we repeated the monopole calculation using the folding model with the interpolated version of the DDG interaction and its associated imaginary Woods-Saxon potential. Although significant changes in the angular distribution appear at large angles, they are rather small in the forward direction. Near the important angle of 1° , the interpolated potential predicts a 20% reduction in cross section (hence a 20% increase in the inferred sum rule depletion). The only way found to avoid the apparent discrepancy

TABLE I. Predicted differential cross sections at some representative forward angles for exciting giant resonances in ^{58}Ni by 240 MeV alpha particles and exhausting 100% of the EWSR limit. The potentials used were determined by fitting the 240 MeV elastic scattering data [24].

Model	0° (mb/sr)	1° (mb/sr)	5° (mb/sr)	Total (mb)
GMR, $Q = -17.42$ MeV				
DP ^a	385	276	56.6	2.94
DDG/WS ^b	398	295	46.1	3.18
BDM3Y1/WS ^c	355	262	41.6	2.79
G194 ^d	286	212	36.0	2.51
G194/WS ^e	350	256	40.4	2.67
GMR, $Q = -20.76$ MeV				
DDG/WS ^b	255	190	29.8	2.02
GQR, $Q = -16.08$ MeV				
DP ^a	95.4	89.3	147	10.6
DDG/WS ^b	68.5	71.3	133	10.5
GQR, $Q = -17.42$ MeV				
DDG/WS ^b	67.8	68.9	115	9.4
GQR, $Q = -20.76$ MeV				
DDG/WS ^b	63.6	63.1	80.8	7.3
GDR, ^f $Q = -17.42$ MeV				
DDG/WS ^b	53.7	44.3	2.56	0.36
GDR, ^f $Q = -20.76$ MeV				
DDG/WS ^b	19.9	16.5	1.16	0.15

^aDeformed potential model, using the Woods-Saxon potential from [24].

^bDensity-dependent Gaussian real interaction and Woods-Saxon imaginary part.

^cDensity-dependent M3Y real interaction and Woods-Saxon imaginary part.

^dDensity-independent Gaussian complex interaction with $t=1.94$ fm, $v=24.9$ MeV, $w=15.0$ MeV.

^eDensity-independent Gaussian real interaction with $t=1.94$ fm, $v=23.5$ MeV, and Woods-Saxon imaginary part.

^fCoulomb excitation only.

when fitting the elastic data at 240 MeV was to use the interpolated value of the DDG interaction but associate it with a very strongly absorbing imaginary potential (even though this is ruled out by the more extensive elastic measurements at 139 and 340 MeV). However, the monopole predictions using this unrealistically strongly absorbing interaction differ only by a few percent at the forward angles.

The effect of the dynamic correction (2.7) on the excitations of low 2^+ and 3^- states was found to be quite large. However, this seems not to be the case for monopole excitations, although the transition potentials (Fig. 6) are changed dramatically in the nuclear interior. Omitting the correction (2.7) increases the cross sections at forward angles by only a few percent, less than 10% when the DDG interaction is used and less than 5% for the BDM3Y1 interaction. The scattering is dominated by contributions from large radii, where the correction is small.

Another fragment of the giant monopole resonance was inferred at a higher excitation energy of 20.76 MeV [9]. Two aspects of this must be considered: The theoretical cross section for a given amplitude α_0^m will be altered because of the

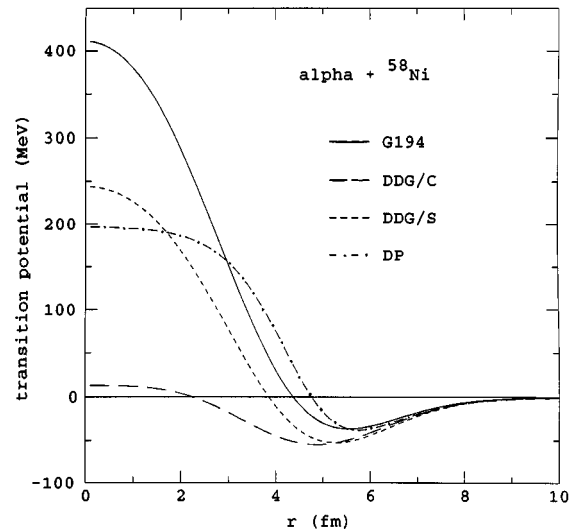


FIG. 6. The real parts of transition potentials for exciting a giant monopole resonance at 17.42 MeV in ^{58}Ni , normalized to unit amplitude α_0^m . That obtained using the deformed potential (DP) model (2.2), based upon the Woods-Saxon potential from [24], is compared to folded potentials obtained using the transition density (2.4) with single-folding Gaussian interactions. G194 is the density-independent Gaussian with a range of $t=1.94$ fm, normalized to reproduce the elastic data at 240 MeV. DDG is the density-dependent Gaussian described in the text; curve C (for ‘‘consistent’’) includes the dynamical correction (2.7) while curve S (for ‘‘simple’’) neglects it.

change in Q value, and the contribution to the energy-weighted sum rule (2.9) from a given α_0^m will increase because of the change in E_x . Put another way, 100% of the sum rule at $E_x=20.76$ MeV would correspond to a smaller amplitude of $\alpha_0^m=0.1259$. The increase in the Q value alone was found to decrease the cross sections uniformly by about 23%, while both effects together reduce the cross sections by one-third (see Table I).

C. Isoscalar giant quadrupole resonance

An appreciable fraction of the giant quadrupole resonance (GQR) was identified centered at $E_x=16.08$ MeV. A deformation length of 0.985 fm would correspond to 100% depletion of the sum rule limit at this energy. We find that the DP model, using the Woods-Saxon potential of [24], gives cross sections about 20% larger than those predicted using the single-folding model with the DDG interaction and the BM form (2.3) for the transition density. Representative values of the cross sections are included in Table I.

The first maximum in the measured angular distribution near 4° is about 90 mb/sr. This corresponds to a sum rule depletion of 44% in the DP model [9], which thus is increased to about 55% if the folding model is used. A comparison with the measured cross sections is shown in Fig. 7.

Fragments of the GQR were also inferred in the spectral peaks centered at 17.42 and 20.76 MeV of excitation. Again the change in Q value affects both the theoretically predicted cross sections and one’s estimate of the depletion of the energy-weighted sum rule limit. For example the theoretical peak cross section for 20.76 MeV of excitation is reduced by

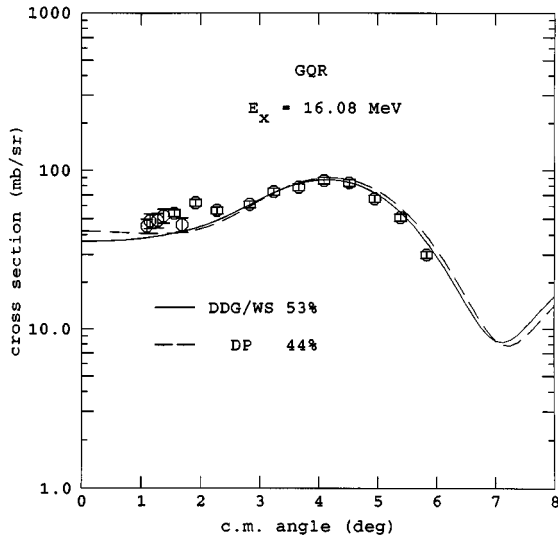


FIG. 7. The predictions of the folding model, with the DDG interaction and a Woods-Saxon imaginary part, for exciting a giant quadrupole resonance at 16.08 MeV in ^{58}Ni , and those given by the deformed potential model (DP), using the Woods-Saxon potential from [24], compared with the measured cross sections [9]. The percentage exhaustion of the energy-weighted sum rule in each case is indicated.

nearly 20% due to the change in Q value alone, while both effects together reduce it by one-third (see Table I). There is also some change in the shape of the angular distribution.

D. Isovector giant dipole resonance

The giant dipole resonance (GDR) also occurs in this giant resonance region of excitation energies. Within our model this is excited only by Coulomb excitation. Then in principle, the GDR cross sections can be inferred from the results of photonuclear experiments [37] and subtracted from the observed inelastic alpha particle spectrum. Unfortunately the photonuclear spectra [dominated by (γ, p) , which is nearly 3 times as strong as (γ, n) in ^{58}Ni] are far from having a simple Lorentzian shape. The (γ, n) spectrum peaks at an energy of about 18 MeV, while the (γ, p) peaks closer to 19 MeV. These energies fall between the 17.42 and 20.76 Gaussian components of the alpha particle spectrum, although because of the large widths of the photopeaks the GDR excitation can be expected to contribute to both components. As a first approximation, we assume these contributions to be equal. Furthermore, in order to obtain some indication of the importance of the GDR excitation, we assume that the sum of these two contributions exhausts the classical sum rule.

The $E1$ Coulomb excitation cross section is very sensitive to the Q value and can vary significantly across the width of the GDR. (For an example, see Table I: Reducing the excitation energy from 20.76 MeV to 17.42 MeV increases the cross section at 0° by a factor of 2.7.) We ignore this complication for our present purpose, and simply evaluate the cross sections at the peak energies of 17.42 and 20.76 MeV. A depletion of 50% of the classical energy-weighted sum rule at these energies in ^{58}Ni corresponds to reduced transition rates of $B(E1)=0.062$ and $0.052 e^2 b$, respectively.

These were used to estimate the Coulomb excitation contributions from the GDR.

V. IMPLICATIONS OF THE 240-MEV DATA

The measured cross sections [9] at the most forward angles for the 17.42 MeV excitation are dominated by any monopole excitation. Consequently they offer the opportunity to determine quite accurately the depletion of the GMR sum rule at this energy, given a reliable model and a realistic assessment of the giant dipole contribution. We believe that the folding model, with the interactions described here, satisfies the criterion of reliability, provided the breathing mode form (2.4) is a good representation of the transition density. One remaining uncertainty is the amount of GDR excitation that is contributing to this component of the spectrum and which also has an angular distribution that peaks at 0° . Rather than trying to find the ‘‘best fit’’ to the angular distribution of the 17.42 MeV component of the spectrum, we contrast the results of assuming no GDR contribution, as in [9], with our crude guess of 50% of the sum rule participating. Without the GDR, use of the single-folding DDG interaction and its accompanying imaginary Woods-Saxon implies a contribution of about 32% of the GMR sum rule limit from this excitation energy. This is compared to the measurements in Fig. 8(a). The double-folding model with the newer and even more realistic BDM3Y1 interaction (see Fig. 5) implies slightly more, about 36%. This is somewhat more than the 22% claimed in [9], where the DP model was used. [We find about 35% when using the DP model with the same optical potential as in [9]. We believe that the difference arises, at least in part, because the authors of [9] did not use the scaling relation (4.1). This reduces the theoretical cross section by a factor of 1.355 and consequently raises the implied sum rule depletion by the same factor.]

The measurements [Fig. 8(a)] do not show the deep, sharp minimum near 3° that is characteristic of a monopole excitation. This can be due, at least in part, to our neglect of any finite angular resolution in the detection system. The acceptance for each bin of data corresponds to a narrow rectangular slit perpendicular to the scattering plane, subtending 4° vertically and 0.44° horizontally. When placed at 0° in the scattering plane, this accepts alpha particles scattered through $\theta=0^\circ$ to $\pm 2^\circ$. The average angle is 1.08° ; hence, this is the smallest angle for which data are shown. As the slit moves away from 0° in the scattering plane, the range of values of θ for which alpha particles are collected, due to the finite length of the slit, decreases rapidly. In principle we should correspondingly average the theoretical cross sections over the same range of θ before comparing with the data. However, we estimate that the averaging has rather little effect, being largely compensated for by the use of average angles for the data; consequently, we have not performed this additional task. The deep minimum in the monopole cross section near 3° is filled in somewhat by averaging, but nowhere near as much as the data show. This is an indication of contributions from other multipoles, especially the quadrupole. As an example, Fig. 8(a) shows the effect of adding 10% of the GQR sum rule, which tends to fill in the minimum although it overshoots at the larger angles. Clearly, determining the precise amount of quadrupole excitation would re-

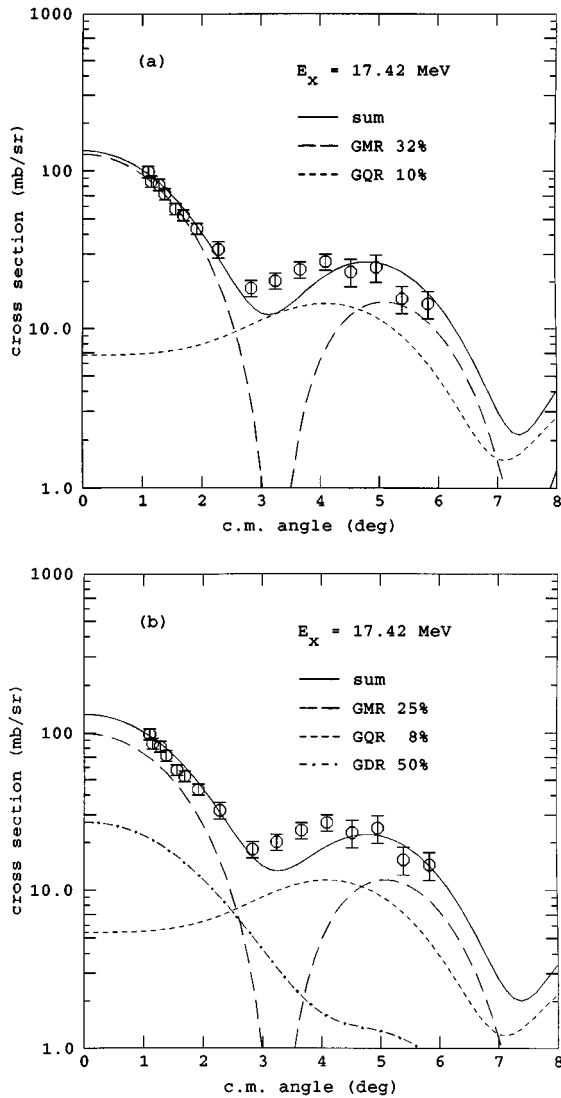


FIG. 8. Examples of fits to the differential cross sections for the 17.42 MeV group excited by 240 MeV alpha particles on ^{58}Ni [9]. The theoretical results were obtained by using folding with the DDG interaction for the real interaction and a deformed Woods-Saxon for the imaginary part. (a) A fit without any contribution from the giant dipole resonance. (b) A fit obtained assuming 50% of the EWSR for the dipole also participates. The percentage exhaustion of the corresponding monopole and quadrupole sum rules is indicated. Note that no angle averaging has been applied to the theoretical cross sections to correct for the finite acceptance of the detectors.

quire careful attention to this averaging.

When we allow 50% of the dipole sum rule to contribute to this 17.42 MeV component, we need less monopole excitation, only about 25% of the sum rule limit, as shown in Fig. 8(b). The quadrupole contribution has also been reduced slightly.

A third peak in the spectral decomposition was obtained a few MeV higher, at $E_x=20.76$ MeV. If we assign 100% of the classical dipole sum to this component (as in [9]), we obtain a nice fit [Figure 9(a)] to the angular distribution within the folding model by adding about 15% of the monopole sum (rather than the 10% found in [9] when using the DP model) and about 10% of the quadrupole sum. However,

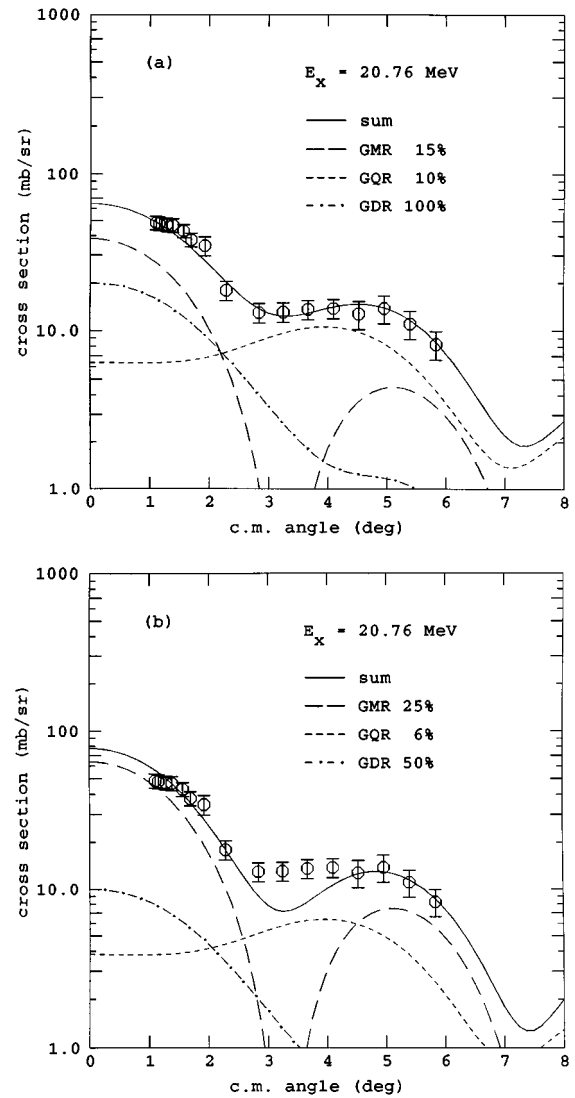


FIG. 9. As for Fig. 8, except for the 20.76 MeV group [9]. (a) Assuming that 100% of the isovector dipole sum rule contributes. (b) Including only 50% of the dipole sum rule. The sum rule percentages for the other multipoles are as indicated. Note that no angle averaging has been applied to the theoretical cross sections to correct for the finite acceptance of the detectors.

as we stressed earlier, the photonuclear measurements indicate that this is an overestimate of the GDR contribution at this excitation energy. If we make our rough guess that 50% is a more realistic figure, we need to increase the monopole estimate to compensate at the most forward angles to about 25%, as shown in Fig. 9(b). There is now a discrepancy between theory and experiment in the region of 3° , similar to that seen for the lower energy component; again, this may be due in part to our neglect of angular averaging to account for finite detector size.

In summary, either assumption about the GDR contributions results in concluding that about one-half of the monopole sum rule limit has been observed in this region of excitation in ^{58}Ni .

VI. SUMMARY AND DISCUSSION

We have studied the application of folded potentials to the elastic and inelastic scattering of 240 MeV alpha particles

from ^{58}Ni and compared the results to those obtained using phenomenological Woods-Saxon potentials and the deformed potential model. The elastic scattering at 139 and 340 MeV was used to indicate acceptable forms for the potentials. This confirmed the need for a density dependence in the folding interaction and for real and imaginary parts with different radial shapes. We used both single folding with a density-dependent Gaussian nucleon-alpha interaction and double folding with a recent density-dependent nucleon-nucleon interaction which has been carefully tailored to reproduce the density and binding energy of normal nuclear matter. We noted a discrepancy between the elastic measurements made at 240 MeV and cross sections predicted by interpolating between the data taken at 139 and 340 MeV.

Comparison of the inelastic scattering predicted by the deformed potential and folding models requires some assumption about the relation between the potential and matter deformation lengths. If we assume these to be equal, we find that the DP model predicts cross sections that are about 20% larger than those given by folding, for quadrupole excitations. This figure increases to about 50% for octupole transitions. However, the two models give much closer results for monopole excitations at the smallest angles, provided the scaling relation (4.1) is assumed for the amplitudes of the breathing mode oscillations.

The dynamical correction (2.7), which is necessary when the folding interaction depends upon the density, can have significant effects on the cross section magnitudes without much change in the angular distributions. It reduces the cross sections by about 25% for $l=2$ and 3, and about 10% for $l=0$.

The measured alpha particle spectrum in the giant resonance region (E_x from 10 to 30 MeV) has been decomposed [9] into three main components centered at excitation energies of 16.08, 17.42, and 20.76 MeV. The component at 16.08 MeV has an angular distribution in good agreement with folding model predictions for quadrupole excitations and a strength corresponding to about 55% of the corresponding energy-weighted sum rule limit. The other two components peak at the smallest angles, consistent with a mixture of dipole and monopole excitations. Although photonuclear experiments show that the giant dipole resonance appears in this region of excitation, and indicate that it should contribute to both components inferred from the alpha particle spectrum, the precise distribution is not clear. As an illustration, we assume that the summed dipole contribution exhausts 100% of the classical sum rule. Two alternatives were tried. One assigned all the strength to the 20.76 MeV component (as assumed in the original analysis [9]). Then the data could be matched by adding 15% of the monopole sum rule and about 10% of the quadrupole one, using the folding model predictions; this is shown in Fig. 9(a). The 17.42 MeV component, shown in Fig. 8(a), could then be matched by assuming 32% of the monopole sum rule accompanied by up to about 10% of the quadrupole sum rule.

The other alternative considered assigned 50% of the dipole sum to each component [see Figs. 8(b) and 9(b)]. Then fitting the small-angle data required about 25% of the monopole sum in each component, together with small amounts (somewhat less than 10% of the sum rule) of quadrupole excitation.

The interesting feature is that while the individual amounts of monopole excitation inferred are sensitive to the distribution assumed for the giant dipole resonance, their sum is not. Consequently, based upon the cross sections measured at the smallest angles, we can assert with some confidence that about one-half of the monopole sum rule limit has been observed in this region of excitation in ^{58}Ni . On the other hand, it is clear that we cannot deduce the quadrupole contributions with any precision, except to say that these two components probably contain between 10% and 20% of the quadrupole sum rule limit. Together with the 55% already assigned to the 16.08 MeV component, this implies that between 65% and 75% of the quadrupole sum has been observed in this region of excitation energies. These conclusions may be compared to the approximately 32% of monopole and about 58% of quadrupole inferred from the original analysis using the deformed potential model [9]. Our results, although somewhat larger, do not differ dramatically. The differences arise from our use of the more realistic folding model and, in the monopole case, from the authors of [9] not using the scaling relation (4.1).

We have not attempted to assign any measure of the uncertainties in our numbers because we have not included precisely the effects of finite detector size, and because they depend upon a number of poorly known features such as the precise amount of dipole excitation present. We do not expect these uncertainties to be large. However, we must stress one particular theoretical uncertainty, namely, the assumption of the BM form (2.3) for the quadrupole transition density and the breathing mode form (2.4) for the monopole one. Some experience with the BM transition density has been reassuring (see, for example, [21]), but the breathing mode version has a much less secure basis. One study, comparing it to the results of RPA structure calculations [10], concluded that it could lead to an underestimate of monopole cross sections (and hence an overestimate of the sum rule depletion).

In contrast to the present results, there are some indications that the excitation of the giant monopole resonance in *heavy* targets by alpha particles, when interpreted in ways similar to those used here, seems to require the exhaustion of more than 100% of the EWSR. This is particularly marked when the folding model is used [4]; for example, ^{208}Pb seems to require at least twice the sum rule limit when excited by 129 MeV alpha particles [38].

Finally, we also draw attention to a study of the excitation of giant resonances in ^{60}Ni by ^{17}O ions [16]. A simple folding model was used. A satisfactory fit to the data [39] for the giant quadrupole resonance at $E_x=16.0$ MeV was obtained, with about 80% of the sum rule. However, the data for the monopole excitations by ^{17}O ions (in other targets, as well as ^{60}Ni) appeared to require in excess of 100% of the monopole sum rule. Possible reasons for this apparent discrepancy are being investigated currently.

ACKNOWLEDGMENTS

We are indebted to Y.-W. Lui and D. H. Youngblood for important communications concerning their data and for providing us with the numerical values. We also thank J. R.

Beene for discussions about the role of the giant dipole resonance. The calculations were made using the nonrelativistic program PTOLEMY; we are indebted to M. Rhoades-Brown for making this available. Oak Ridge National Laboratory is managed by Lockheed Martin Energy Research Corporation for the U.S. Department of Energy under Contract No. DE-

AC05-96OR22464. Theoretical nuclear physics research at the University of Tennessee is supported by the U.S. Department of Energy through Contract Nos. DE-FG05-93ER40770 and DE-FG05-87ER40461. The research at Chung Yuan Christian University is supported by the National Science Council of the ROC.

-
- [1] H. J. Lu, S. Brandenburg, R. de Leo, N. M. Harakeh, T. D. Poelheken, and A. van der Woude, *Phys. Rev. C* **33**, 1116 (1986).
- [2] Y.-W. Lui, J. D. Bronson, D. H. Youngblood, Y. Toba, and U. Garg, *Phys. Rev. C* **31**, 1643 (1985).
- [3] D. H. Youngblood, P. Bogucki, J. D. Bronson, U. Garg, Y. -W. Lui, and C. M. Rozsa, *Phys. Rev. C* **23**, 1997 (1981).
- [4] F. E. Bertrand, G. R. Satchler, D. J. Horen, J. R. Wu, A. D. Bacher, G. T. Emery, W. P. Jones, D. W. Miller, and A. van der Woude, *Phys. Rev. C* **22**, 1832 (1980).
- [5] G. Duhamel, M. Buenerd, P. de Saintignon, J. Chauvin, D. Lebrun, Ph. Martin, and G. Perrin, *Phys. Rev. C* **38**, 2509 (1988).
- [6] F. E. Bertrand, G. R. Satchler, D. J. Horen, and A. van der Woude, *Phys. Lett.* **80B**, 198 (1979).
- [7] U. Garg, P. Bogucki, J. D. Bronson, Y.-W. Lui, C. M. Rozsa, and D. H. Youngblood, *Phys. Rev. C* **25**, 3204 (1981).
- [8] D. H. Youngblood and Y.-W. Lui, *Phys. Rev. C* **44**, 1878 (1991).
- [9] D. H. Youngblood, H. L. Clark, and Y.-W. Lui, *Phys. Rev. Lett.* **76**, 1429 (1996).
- [10] Ph. Chomaz, Tüna Suomijärvi, N. Van Giai, and J. Treiner, *Phys. Lett. B* **281**, 6 (1992).
- [11] G. R. Satchler, *Direct Nuclear Reactions* (Oxford University Press, Oxford, 1983).
- [12] G. R. Satchler, *Nucl. Phys.* **A540**, 533 (1992).
- [13] G. R. Satchler, *Nucl. Phys.* **A472**, 215 (1987).
- [14] H. Uberall, *Electron Scattering from Complex Nuclei* (Academic Press, New York, 1971), Vol. B.
- [15] G. R. Satchler, *Part. Nucl.* **5**, 105 (1973).
- [16] D. J. Horen, J. R. Beene, and G. R. Satchler, *Phys. Rev. C* **52**, 1554 (1995).
- [17] V. R. W. Edwards and B. C. Sinha, *Phys. Lett.* **37B**, 225 (1971).
- [18] J. R. Beene, D. J. Horen, and G. R. Satchler, *Phys. Rev. C* **48**, 3128 (1993).
- [19] J. R. Beene, D. J. Horen, and G. R. Satchler, *Nucl. Phys.* **A596**, 137 (1996).
- [20] J. R. Beene, D. J. Horen, and G. R. Satchler, *Phys. Lett. B* **344**, 67 (1995).
- [21] D. J. Horen, G. R. Satchler, S. A. Fayans, and E. L. Trykov, *Nucl. Phys.* **A600**, 193 (1996).
- [22] A. Budzanowski, H. Dabrowski, L. Freindl, K. Grotowski, S. Micek, R. Planeta, A. Strzalkowski, M. Bosman, P. Leleux, P. Macq, J. P. Meulders, and C. Pirart, *Phys. Rev. C* **17**, 951 (1978).
- [23] A. M. Bernstein, *Adv. Nucl. Phys.* **3**, 325 (1969).
- [24] H. L. Clark, Y.-W. Lui, and D. H. Youngblood, *Nucl. Phys.* **A589**, 416 (1995).
- [25] E. Friedman and C. J. Batty, *Phys. Rev. C* **17**, 34 (1978); E. Friedman, H. J. Gils, H. Rebel, and Z. Majka, *Phys. Rev. Lett.* **41**, 1220 (1978).
- [26] D. K. Srivastava and H. Rebel, *J. Phys. G* **10**, L127 (1984).
- [27] M. El-Azab Farid and G. R. Satchler, *Nucl. Phys.* **A481**, 542 (1988).
- [28] Dao T. Khoa and W. von Oertzen, *Phys. Lett. B* **342**, 6 (1995).
- [29] H. De Vries, C. W. De Jager, and C. De Vries, *At. Data Nucl. Data Tables* **36**, 495 (1987).
- [30] Dao T. Khoa and W. von Oertzen, *Phys. Lett. B* **304**, 8 (1993).
- [31] L. Ray, *Phys. Rev. C* **19**, 1855 (1979).
- [32] D. A. Goldberg, S. M. Smith, and G. F. Burdzik, *Phys. Rev. C* **10**, 1362 (1974).
- [33] B. Bonin, N. Alamanos, B. Berthier, G. Bruge, H. Faraggi, J. C. Lugol, W. Mittag, L. Papineau, A. I. Yavin, J. Arvieux, L. Farvacque, M. Buenerd, and W. Bauhoff, *Nucl. Phys.* **A445**, 381 (1985).
- [34] U. Atzrott, P. Mohr, H. Abele, C. Hillenmayer, and G. Staudt, *Phys. Rev. C* **53**, 1336 (1996).
- [35] S. Raman, C. H. Malarkey, W. T. Milner, C. W. Nestor, and P. H. Stelson, *At. Data Nucl. Data Tables* **36**, 1 (1987).
- [36] R. H. Spear, *At. Data Nucl. Data Tables* **42**, 55 (1989).
- [37] B. L. Berman and S. C. Fultz, *Rev. Mod. Phys.* **47**, 713 (1975).
- [38] D. H. Youngblood (private communication).
- [39] R. Liguori Neto, P. Roussel-Chomaz, L. Rochais, N. Alamanos, F. Auger, B. Fernandez, J. Gastebois, A. Gillibert, R. Lacey, A. Miczaika, J. Barrette, S. K. Mark, R. Turcotte, Y. Bluenfeld, N. Frascaria, J. P. Garron, J. C. Roynette, J. A. Scarpaci, A. Van der Woude, and A. M. Van der Berg, *Nucl. Phys.* **A560**, 733 (1993).